

Article

Fourier and Chirp-Z Transforms in the Estimation Values Process of Horizontal and Vertical Synchronization Frequencies of Graphic Displays

Ireneusz Kubiak *  and Artur Przybysz

Department of Electromagnetic Compatibility, Military Communication Institute—State Research Institute, 05-130 Zegrze Poludniowe, Poland; a.przybysz@wil.waw.pl

* Correspondence: i.kubiak@wil.waw.pl

Abstract: The electromagnetic protection of IT devices includes a number of organizational and technical measures aimed at ensuring control over radiated and conducted revealing emissions. This is of particular importance for ensuring information security in wireless communication and the processing of data presented in graphic form. In each of these cases, the occurring electromagnetic emissions pose the risk of a lack of electromagnetic immunity to the so-called eavesdropping process based on forming revealing emissions. Included in the elements of the security chain preventing electromagnetic eavesdropping on wireless communication and the devices building such systems are activities related to the determination of the Technical Device Security Level (TDSL) or its class. The above is related to the performance of electromagnetic emissions tests and identifying which of them must be treated as revealing emissions, which are only disturbances and do not threaten the security of the processed information. It is intuitively understandable that it is particularly important to ensure the security of interfaces that process video data. The nature of the electromagnetic emission signals generated by these interfaces means that the related information can be intercepted with the use of relatively simple methods, and under favorable circumstances even with the use of a receiving device not very technologically advanced. In the case of the electromagnetic safety assessment of video devices, common practice is therefore activities aimed at reconstructing information related to the video signal. This requires the parameters of the reconstructed image appropriate for the eavesdropped device operation mode and the conditions of recording the revealing emission signals to be determined. The article presents the results of works related to the analysis of the possibility of using spectral analysis methods (Fast Fourier FFT transform and Chirp-Z transform) to automate the process of determining the above-mentioned parameters in the case of reproducing images from emission signals recorded by using the ADC analog-to-digital converter.

Keywords: Fourier transform; Chirp-Z transform; wireless communication; rasterization; graphic display; reveal emission; protection of information; electromagnetic eavesdropping; AWGN noise



Citation: Kubiak, I.; Przybysz, A. Fourier and Chirp-Z Transforms in the Estimation Values Process of Horizontal and Vertical Synchronization Frequencies of Graphic Displays. *Appl. Sci.* **2022**, *12*, 5281. <https://doi.org/10.3390/app12105281>

Academic Editor: Christos Bouras

Received: 24 April 2022

Accepted: 22 May 2022

Published: 23 May 2022

Publisher's Note: MDPI stays neutral with regard to jurisdictional claims in published maps and institutional affiliations.



Copyright: © 2022 by the authors. Licensee MDPI, Basel, Switzerland. This article is an open access article distributed under the terms and conditions of the Creative Commons Attribution (CC BY) license (<https://creativecommons.org/licenses/by/4.0/>).

1. Introduction

The protection of information, understood as electromagnetic immunity to an electromagnetic infiltration process, is very important in the case of wireless communication. Very often, wireless communication is based on electronic devices equipped with graphic displays presenting the protected data. Their processing is protected by the use of cryptographic techniques. However, the display process is based on explicit, human-understood data. Then, they become a source of revealing emissions that can be used in the process of non-invasive acquisition [1–3].

The presentation in the form of an image of information processed in a device using the raster graphics technique for this purpose requires imaging (rasterization) parameters to be identified that enable the transformation of one-dimensional information signals (video

signals) into a two-dimensional matrix with dimensions corresponding to the parameters of the displayed image [4–6]. Based on the example of a typical monitor, it can be stated that its screen is made of points (pixels) capable of emitting radio waves, forming a matrix consisting of W rows and K columns, and the manner of this emission is determined by the video signal (a source of reveal emission).

Based on the data contained in [7], the most important display parameters (image dimensions) of the information on the monitor can be given for selected operating modes (Table 1).

Table 1. Catalog parameter values of the rasterization for selected monitor operating modes (Data from [7]).

| Operating Mode of Display | Total Number of Image Lines | Total Number of Pixels in Line | Pixel Frequency [MHz] | Horizontal Sync Frequency [kHz] |
|---------------------------|-----------------------------|--------------------------------|-----------------------|---------------------------------|
| 640 × 480/60 Hz | 525 | 800 | 25.175 | 31.469 |
| 800 × 600/60 Hz | 628 | 1056 | 40.000 | 37.789 |
| 1024 × 768/60 Hz | 806 | 1344 | 65.000 | 48.363 |
| 1280 × 1024/60 Hz | 1066 | 1688 | 108.000 | 63.981 |
| 1366 × 768/60 Hz | 798 | 1792 | 85.500 | 47.712 |
| 1440 × 900/60 Hz | 934 | 1904 | 106.500 | 55.935 |
| 1600 × 900/60 Hz | 1000 | 1800 | 108.000 | 60.000 |
| 1600 × 1200/60 Hz | 1250 | 2160 | 162.000 | 75.000 |
| 1920 × 1080/60 Hz | 1125 | 2200 | 148.500 | 67.500 |
| 2048 × 1152/60 Hz | 1200 | 2250 | 162.000 | 72.000 |
| 4096 × 2160/60 Hz | 2222 | 4176 | 556.744 | 133.320 |

In the case of generating the image in the device, these parameters are known, and the horizontal and vertical synchronization signals generated by the graphics card ensure correct imaging, even in the case of slight changes in their values. The situation is different in the case of reconstructing the information from the revealing signals. On the receiving side, without precise measurements that often require interference with the interior of the eavesdropped device, only the approximate values of the displaying parameters can be known. They are sufficient to display the information reproduced from signals with positive value of a signal to noise ratio (SNR). However, they are of little use in the case of very small SNR and the need to improve it using the coherent summation method. Then, the determined accuracy of the aforementioned parameters must be very high. Otherwise, the summation of the successive images obtained from the same revealing emission (RU) causes a deterioration of the image quality, not an improvement thereof.

The phenomena of the formation of revealing emissions described in scientific publications and the possibility of using them in the process of electromagnetic infiltration are limited to studies of radiated and conducted emissions [8–12]. There are presented results of analyses of the impact of various solutions on the effectiveness of electromagnetic protection. The sources of the revealing emissions in the form of monitors, displays of multifunction devices or VoIP terminals and communication interfaces are analyzed [13]. Methods of data acquisition and attempts to present them graphically are presented [14–16]. There is no information about the impact of the accuracy of determining the image raster parameters (line length of the reconstructed image) on its quality and the possibility of efficiently applying the image summation method to improve the signal-to-noise ratio. Another widely analyzed area is the confirmation of the existence of revealing emissions, the analysis of the dependence of the processed signal structures on the efficiency of the emission source and an attempt to reconstruct information without indicating detailed

raster parameters for data in graphic form [17–19]. It should not be forgotten that the revealing emission signals are very noisy signals and the images reproduced on their basis often contain only the outlines of the data sought. This is the result of the use of various solutions counteracting the effectiveness of the electromagnetic infiltration process, including in the form of electromagnetic screens [20] or noise generators [21]. Then, the accuracy of the aforementioned rastering parameters is very important, for example, for the successful use of coherent image summation algorithms, the result of which will be an improving the image quality and the readability of the data contained therein.

Determining the signal raster parameters on the basis of catalog data or the results of previous measurements of analogous IT devices may be burdened with an error, preventing the reproduction of the image in a way that allows for unambiguous identification of the analyzed signal by sight method. In the case of signals with positive SNR, the basing on the catalog data may be sufficient. The refinement of the software raster parameter values can be made based on the method of visual correction of image geometry distortions, i.e., by manually specifying the raster parameter values with simultaneous observation of the impact of their change on the quality of the reproduced image. However, in the case of sources of revealing emission signals, the parameters of which are unknown (especially in the case of highly noisy signals or those whose manufacturers do not provide such parameters, e.g., printers), it becomes necessary to have a tool that enables raster parameters to be determined in an automatic manner.

The risk related to the loss of information may also apply to IoT devices equipped with graphic displays. Such devices can present data related to the operation of video intercoms, images from surveillance cameras, access manipulators, etc. [22,23]. They can also be SmartOffice devices presenting the multitude of data related to the company's operations. Each display of such devices that process graphical data may become a source of undesirable emissions and constitute a risk of security [24,25].

The aim of the article is to present the issues related to the influence of the accuracy of determining the raster parameters of an image on the quality of its reconstruction. Examples of rough estimation of image line length (Fourier transform) and its influence on the quality of the reconstructed image are presented. At the same time, the consequences of such a phenomenon on the possibility of using coherent summation to improve the signal-to-noise ratio are indicated. The emerging phenomenon forces the search for a more precise method of determining the length of the lines of the reconstructed image, which will affect the quality and thus the legibility of the data contained in the reconstructed image. One of the methods is the Chirp-Z transform [26], also written as CZT [27–29], which allows for the analysis of a selected fragment of the signal spectrum obtaining greater spectral resolution and more precise indication of the frequency value which corresponds to a local maximum of the spectrum.

2. Information Reproducing by Using a Real Analog-to-Digital Converter (ADC)

The assessment of the safety of emissions of devices intended for processing graphic information requires the determination of the possibility of their reconstruction from the recorded signals of revealing emissions. For this purpose, the image rastering technique is used, which requires the determination of its geometrical dimensions (width, height), taking into account the conditions resulting from the applied method of recording and visualizing these signals (sampling). In physical devices, the timing signals used for imaging are produced with a finite accuracy; moreover, the recording devices have a finite number of available sampling frequencies. For this reason, the width of the image (line length) to be taken into account in the rastering process is not expressed as an integer. The accuracy of its determination, however, is important in the case of signals for which, due to low SNR values, obtaining a clear image requires the use of coherent summation techniques. In this case, obtaining the accuracy of determining the row length at the level of 10^{-4} using the FFT method requires transform calculations to be performed on sets of samples with sizes of the order of TB, which results in a significant extension of the

computation time (several dozen–several hundred seconds) and the need to use large RAM memory resources (representation 64-bit).

The use of the simple Fourier transform to determine the raster parameters is therefore a computationally inefficient process. The determined amplitude spectrum will largely remain unused. A more useful solution is the use of the CZT transform, which makes it possible to determine the spectrum of the signal only in a given frequency sub-range, with the required accuracy determined using a much smaller number of samples.

The simulation tests were carried out with the use of two work stations:

- Computer with 8 GB of DDR3-1333 RAM, Intel Pentium Core2Quad Q8300 processor running at 2.5 GHz. For such a hardware platform, in a 64-bit Windows environment, the maximum samples string length for FFT transform calculations was 2^{28} (256 MS).
- Computer equipped with 64 GB of DDR4-2666 RAM memory, Intel Pentium i9-10900X processor with a clock frequency of 3.7 GHz. For such a hardware platform, the maximum samples string length for FFT transform calculations was 2^{31} (2 GS).

The average computation times (for 10 repetitions) of a single transform of a given length are shown in Table 2. The limiting values of the transformation length require computer memory management, i.e., resource allocation for computations. Out of memory errors occur when the amount of RAM is too low. The tests were limited to signals obtained analytically from the Word editor window image, and the accuracy of determining the parameters of rastering of R_H line length and the number of L_V lines for the use of the FFT and CZT transforms were compared.

Table 2. Average FFT and CZT transform computation time for exemplary hardware platforms.

| Length of the Sample String | Pentium i9-10900X | | Pentium C2Q Q8300 | |
|-----------------------------|------------------------------|------------------------------|------------------------------|------------------------------|
| | Calculation Time for FFT [s] | Calculation Time for CZT [s] | Calculation Time for FFT [s] | Calculation Time for CZT [s] |
| 2^{22} | 0.06 | 2.74 | 0.19 | 15.26 |
| 2^{23} | 0.12 | 5.82 | 0.43 | 34.07 |
| 2^{24} | 0.22 | 12.61 | 0.94 | 74.54 |
| 2^{25} | 0.43 | 26.51 | 1.96 | 298.82 |
| 2^{26} | 0.88 | 58.81 | 4.48 | out of memory |
| 2^{27} | 1.51 | 119.05 | 82.91 | out of memory |
| 2^{28} | 2.05 | 272.42 | 412.46 | out of memory |
| 2^{29} | 7.75 | out of memory | out of memory | out of memory |
| 2^{30} | 15.78 | out of memory | out of memory | out of memory |
| 2^{31} | 115.44 | out of memory | out of memory | out of memory |
| 2^{32} | out of memory | out of memory | out of memory | out of memory |

In the case of recording the revealing emission signals with an ADC, a specific sampling rate may be used. For example, the PDA-1000 8-bit analog-to-digital converter card, manufactured by Signatec, offers a signal sampling rate equal 1 GS/s, which can be reduced by dividing the card’s clock frequency in the range from 2 to 1024. Assuming the perfect execution of both the transducer card and the graphics card elements and assuming that the minimum sampling frequency should be at least equal to the “pixel frequency”, for the previously selected monitor operating modes (Table 1) and the ADC card the values of the acquisition and screening parameters of the EU signals were obtained (Table 3).

Table 3. Rasterization parameters in the case of signal recording by using an ADC card.

| Operating Mode of Display | Pixel Frequency [MHz] | Sampling Rate [MHz] | Vertical Synchronization Frequency [kHz] | Estimated Number of Pixels on the Line |
|---------------------------|-----------------------|---------------------|--|--|
| 640 × 480/60 Hz | 25.175 | 31.25 | 31.500 | 992.0634921 |
| 800 × 600/60 Hz | 40.000 | 62.50 | 37.789 | 1653.920453 |
| 1024 × 768/60 Hz | 65.000 | 125.00 | 48.363 | 2584.620474 |
| 1280 × 1024/60 Hz | 108.000 | 125.00 | 63.981 | 1953.705006 |
| 1366 × 768/60 Hz | 85.500 | 125.00 | 47.712 | 2619.885983 |
| 1440 × 900/60 Hz | 106.500 | 125.00 | 55.935 | 2234.736748 |
| 1600 × 900/60 Hz | 108.000 | 125.00 | 60.000 | 2083.333333 |
| 1600 × 1200/60 Hz | 162.000 | 250.00 | 75.000 | 3333.333333 |
| 1920 × 1080/60 Hz | 148.500 | 250.00 | 67.500 | 3703.703704 |
| 2048 × 1152/60 Hz | 162.000 | 250.00 | 72.000 | 3472.222222 |
| 4096 × 2160/60 Hz | 556.744 | 1000.00 | 133.320 | 7500.750075 |

The information in Table 3 shows that the length of the line (number of pixels in a line) of the reconstructed image is not expressed by the total number of pixels, and the accuracy of its reproduction is important in the process of summing up the images. The authors' experience shows that in this case this value should be determined with an accuracy of 10^{-4} . An additional difficulty is the fact that these values can significantly differ for individual graphics cards, and they can additionally fluctuate during the work of a specific copy, as well as during electromagnetic wiretapping. This phenomenon significantly hampers the possibility of correct determination of the image line length from the point of view of the expected effect of improving its quality for coherent summation [30,31].

3. Time-Frequency Characteristics of Video Signals

The video signal generated by the graphic card is sent to the monitor in a serial manner. Correct mapping of the video signal into the image is ensured by information that determines the parameters of horizontal and vertical synchronizations (the length of the image line and the number of lines in the image). The historical background related to the principles of operation of cathode ray tubes means that even modern light-emitting diode (LED) monitors operate in accordance with the rules of image framing developed for Cathode-Ray Tube (CRT) monitors, which, in the transmitted video signal require appropriate gaps to be reserved, once necessary for proper positioning of the electron beam. This property can be helpful in determining rasterization parameters with unknown work parameters of the monitor (display), which is an element of electromagnetic eavesdropping.

Examples of dependencies for the 640 × 480/60 Hz mode are presented in Figure 1. In inactive state, both sync signals are high (logical "1"). The display of the line (row) begins with the appearance of the horizontal sync pulse about a duration 3.81 μs (96 cycles of pixel clock). However, before the transmission of the video signals corresponding to individual pixels in the line begins, it is necessary to return the electron beam to the beginning of the line (48 + 16 clock cycles of the pixel = 1.91 μs + 0.64 μs). Each line is displayed in time 25.42 μs (640 pixel clock cycles). The total time needed to display one line is 31.77 μs (96 + 48 + 640 + 16 = 800 cycles of the pixel clock). The same applies to the vertical sync signals. The sync pulse itself lasts 63.6 μs, and the total time needed to display the image once is 16,683 μs, while the display of 480 image lines alone takes 15,253 μs. The time to return to the beginning of the image is 1367 μs.

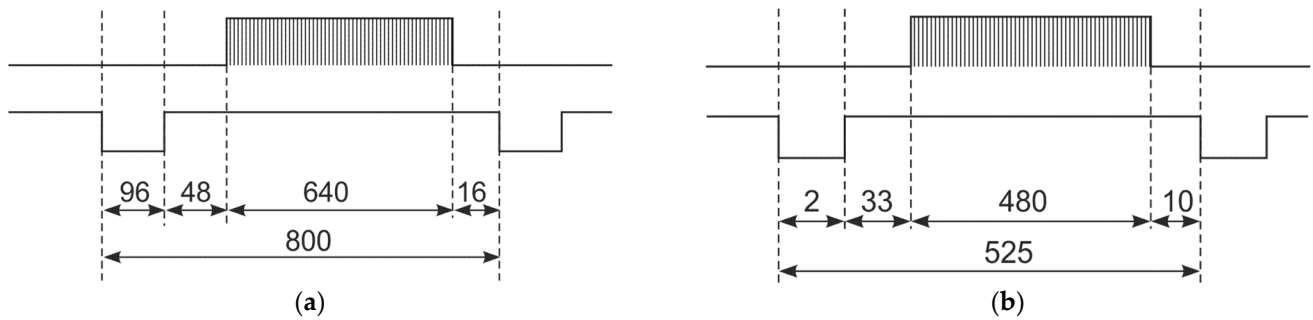


Figure 1. Timing relationships between video signals and (a) horizontal and (b) vertical sync signals for VGA monitor (video graphics array) operating in 640 × 480/60 Hz mode.

Video signals processed in imaging devices using the raster technique are characterized by a characteristic order. Video data are sent from the source to the receiver at strictly defined time intervals and in strictly defined “portions”. Horizontal and vertical sync data signals form characteristic frames, which are the result of multiplication of signals: sampled information, horizontal sync and vertical sync [2,32,33].

The spectrum of the product of the signals is equal to the convolution of the spectra of the component signals. Taking into account the above in the spectrum of the reveal signal coming from the video signal, spectral lines will appear corresponding to the frequencies of the sync signals.

To illustrate the above statement, the amplitude spectra of two models of the revealing emission signals obtained in an analytical manner, i.e., from reading the pixel values corresponding to the RED channel information of the images stored in the form of the BMP file, were determined. Two images, presented in Figure 2, were analyzed: vertical black and white stripes 8 pixels wide and the screen of the MS Word editor. The above can be compared with the case of displaying data on the displays of wireless communication devices. The lack of knowledge of the display operation mode requires carrying out the analyses necessary to obtain data about the parameters of the displayed image in order to recreate it from the recorded revealing emission.

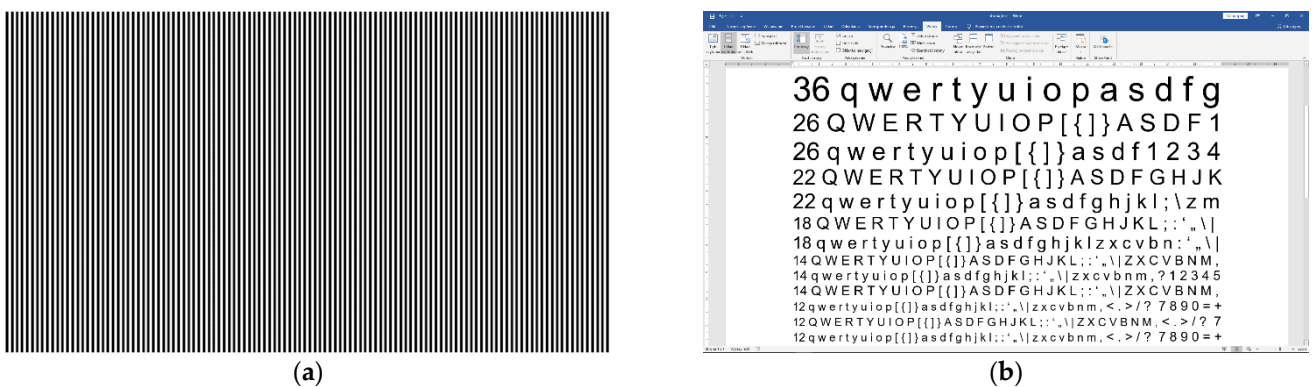


Figure 2. Test images: (a) 8 × 8 vertical stripes and (b) a window of MS Word editor.

The images sizes correspond to a screen resolution of 1920 × 1080 pixels. Based on the information contained in [7], models of video signals corresponding to the vertical refresh rate of 60 Hz were created. Under these conditions, the horizontal frequency is 67.5 kHz and the pixel frequency is 148.5 MHz. In order to map the characteristics of the real propagation channel (radiated type) of the reveal signals, the obtained signal was subjected to the differentiation operation. The amplitude spectra of the above-mentioned signals determined with the use of the FFT transform were shown in Figures 3–5. It was assumed that the signal was sampled at 297 MS/s, and 256 MS samples were included in the calculations.

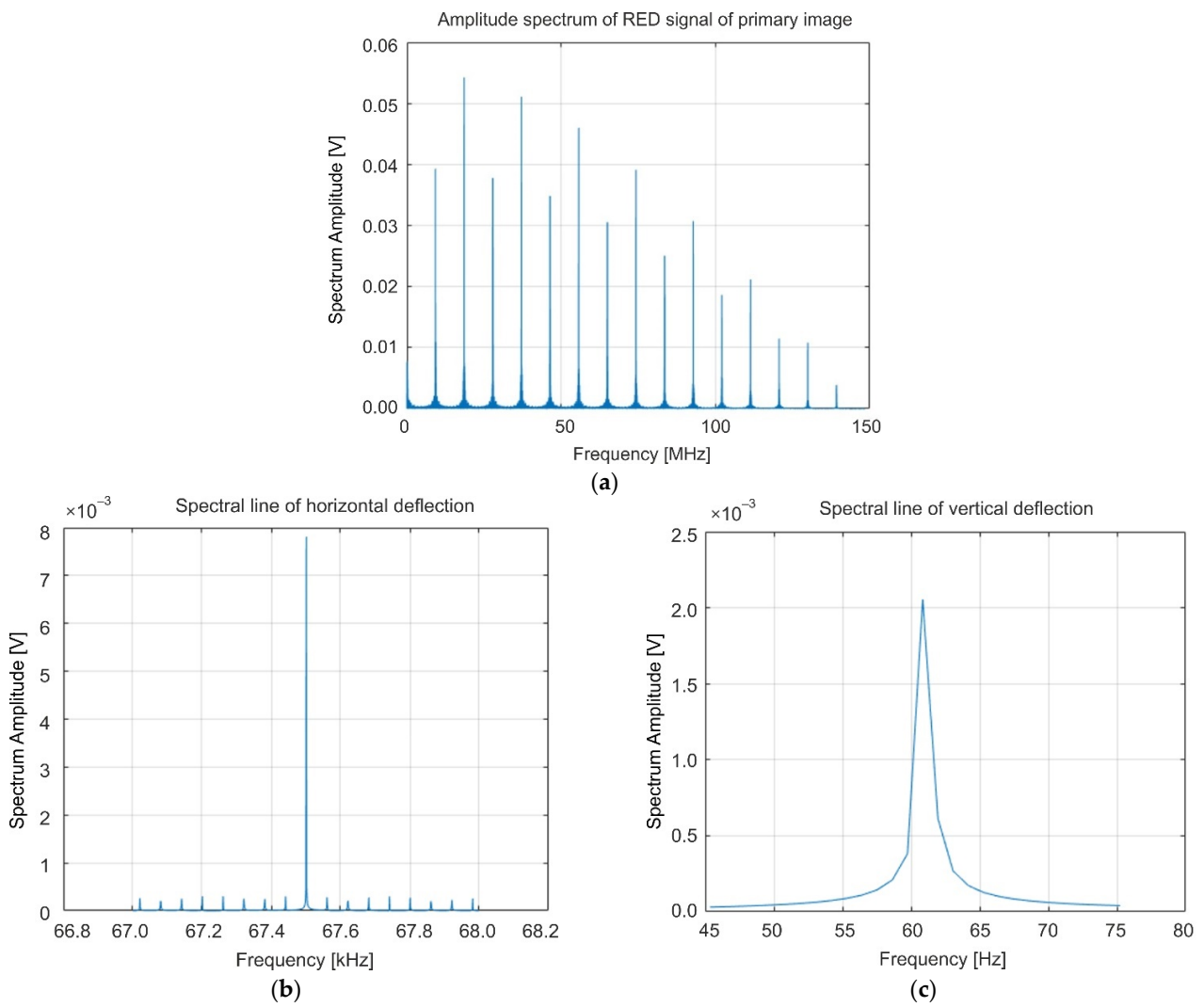


Figure 3. (a) Amplitude spectrum of the test signal (strips 8×8) and magnification of its fragments corresponding to the (b) horizontal and (c) vertical sync frequencies.

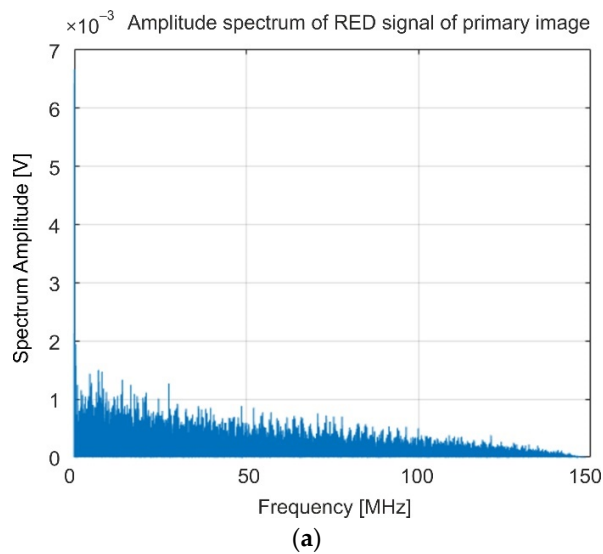


Figure 4. Cont.

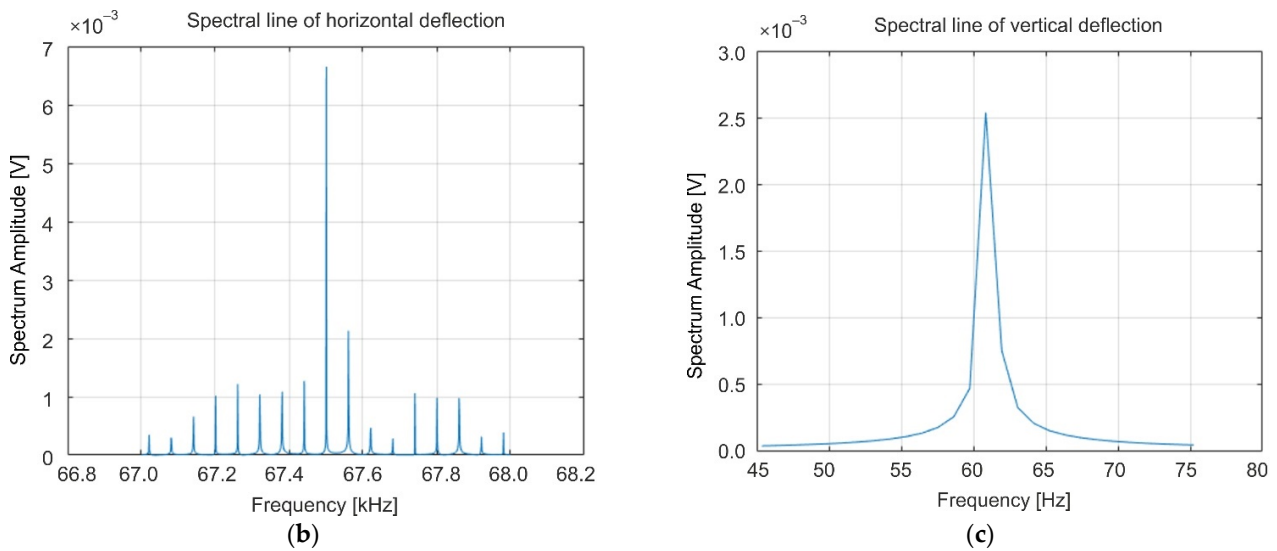


Figure 4. (a) Amplitude spectrum of the test signal (window of MS Word editor) and magnification of its fragments corresponding to the (b) horizontal and (c) vertical sync frequencies.

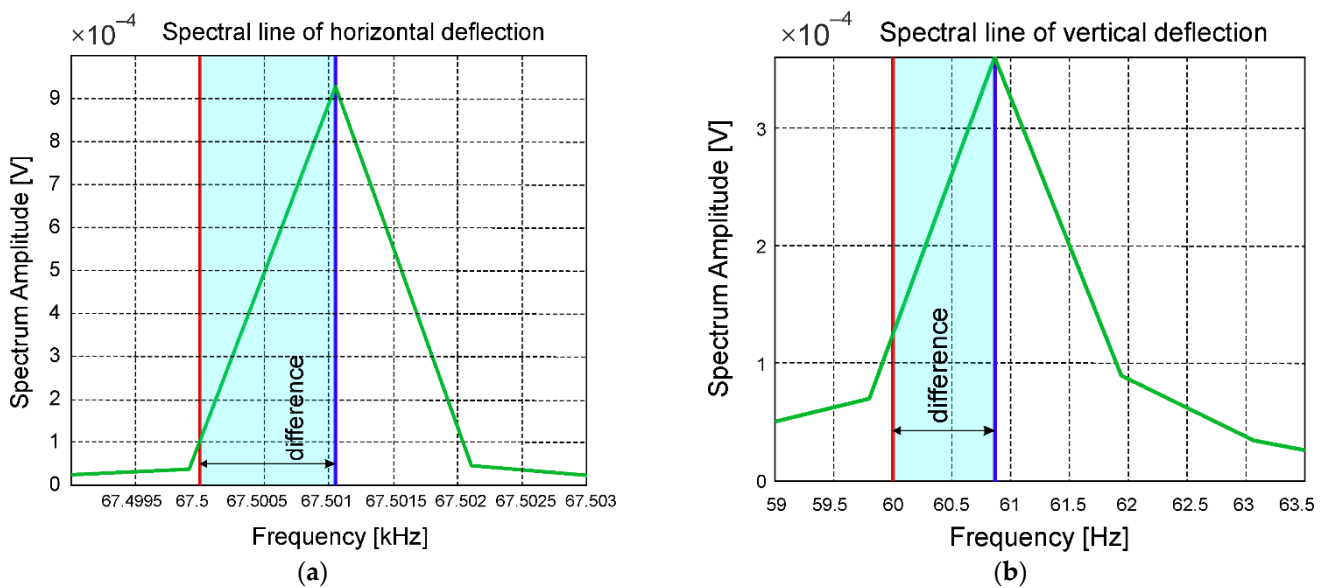


Figure 5. Magnification of the fragments of the amplitude spectrum corresponding to the (a) horizontal and (b) vertical sync frequencies.

When analyzing the above-presented fragments of the spectrum corresponding to the horizontal and vertical spectral lines, it can be noticed that even in the case of a signal built strictly according to the recommendations [7], the finite accuracy of the calculations causes the values of these frequencies determined with the use of the FFT transform to differ from the assumed ones. This indicates the need to look for solutions that can approximate the values of the above parameters with greater accuracy [34]. At the same time, it should allow to use of coherent summation with a greater multiplicity. Then, it will be possible to obtain an improvement in the value of the SNR.

4. Determination of Rasterization Parameter Values

4.1. FFT Transform

The horizontal and vertical frequencies values can be determined by analyzing the spectrum of the recorded video signal (or the revealing signal). Using the FFT transform, it

is possible to determine the position of the spectrum lines corresponding to the image line length and their number in the image [35–37].

The resolution of the FFT transform is determined by the ratio of the sampling frequency f_s to the number of samples N being subject to analysis.

$$\Delta f = \frac{f_s}{N} \tag{1}$$

As mentioned earlier, the operation of recreating the actual line length should be performed with accuracy to the fourth decimal place. In the case of, e.g., monitors operating in the modes and with the parameters specified in Table 1, let f_H denote the value of the horizontal synchronization frequency corresponding to the actual length of the image line, f_{H1} denote the value of the horizontal synchronization frequency corresponding to the actual length of the image line reduced about value 0.01, and f_{H2} denote the value of the horizontal synchronization frequency corresponding to the actual image line length increased about value 0.01. According to the formula:

$$\Delta f_H = f_{H1} - f_H = f_H - f_{H2}, \tag{2}$$

the accuracy values of determining the horizontal synchronization frequency were obtained (Table 4).

Table 4. Determination of the required spectrum resolution for the FFT.

| Operating Mode of Display | Sampling Rate [MHz] | Real Number of Pixels in the Line | f_H [Hz] | f_{H1} [Hz] | f_{H2} [Hz] | Δf_H [Hz] |
|---------------------------|---------------------|-----------------------------------|-------------|---------------|---------------|-------------------|
| 640 × 480/60 Hz | 31.25 | 993.0408 | 31,468.9991 | 31,469.3160 | 31,468.6822 | 0.3169 |
| 1366 × 768/60 Hz | 125.00 | 2619.8860 | 23,855.9998 | 23,856.0909 | 23,855.9088 | 0.0911 |
| 1600 × 900/60 Hz | 125.00 | 2083.3333 | 60,000.0010 | 60,000.2890 | 59,999.7130 | 0.2880 |
| 1920 × 1080/60 Hz | 250.00 | 3703.7037 | 67,500.0001 | 67,500.1823 | 67,499.8178 | 0.1823 |

Taking into account the above-specified accuracy of determining the horizontal synchronization frequency, it is possible to determine the required number of signal samples necessary to determine the amplitude spectrum by using the FFT (Table 5).

Table 5. Determination of the required number of samples for the FFT.

| Operating Mode of Display | Sampling Rate [MHz] | Δf_H | Requirement Number of Samples |
|---------------------------|---------------------|--------------|-------------------------------|
| 640 × 480/60 Hz | 31.25 | 0.3169 | 98,612,011 |
| 1366 × 768/60 Hz | 125.00 | 0.0911 | 686,377,646 |
| 1600 × 900/60 Hz | 125.00 | 0.2880 | 434,025,681 |
| 1920 × 1080/60 Hz | 250.00 | 0.1823 | 1,371,738,407 |

Based on Table 5, it can be concluded that the use of a simple FFT transform to determine the values of raster parameters would require the use of large computing resources and operating on very large data sets. It should be additionally taken into account that the performance of FFT calculations at a certain level of accuracy requires the use of a representation of numbers in the double (64-bit) format, so the data sets in the PC memory used for calculations are 8 times larger than the required number of samples presented in Table 5. It should be noted that the Fourier transform applies to the entire frequency range of the analyzed signal. In the most cases, this is an uneconomical process. In addition, the so-called frequency resolution of the Fourier transform, i.e., the smallest detectable difference between the two spectral components, is insufficient. Very often,

an important frequency range that should be analyzed is a relatively narrow frequency sub-range. In the discussed issue, these are the ranges concentrated around the horizontal or vertical synchronization frequencies. Therefore, algorithms should be used to determine the signal spectrum for a given frequency range. An example of such an algorithm is the Chirp-Z transform [26–29].

4.2. Chirp-Z Transform (Chirp Transform)

Fourier transform of the N -element sequence of signal samples $x(n)$, where $0 \leq n \leq N - 1$, determined for $(M - 1)$ normed frequency values $f_k = f_0 + k \cdot \Delta f$, where $0 \leq k \leq M - 1$, is determined by the relationship [26]:

$$X(k) = \sum_{n=0}^{N-1} x(n) \cdot e^{-j2\pi f_k n}. \tag{3}$$

Replacing:

$$A = e^{-j2\pi f_0} \tag{4}$$

and

$$W = e^{-j2\pi \Delta f / 2} \tag{5}$$

there is obtained:

$$X(k) = \sum_{n=0}^{N-1} x(n) A^n W^{2kn}. \tag{6}$$

Taking into account:

$$2kn = n^2 + k^2 - (k - n)^2, \tag{7}$$

Fourier transform can be written as:

$$X(k) = W^{k^2} \sum_{n=0}^{N-1} [x(n) A^n W^{n^2}] W^{-(k-n)^2}. \tag{8}$$

The above expression corresponds to the convolution of two signals: $y_1(n) = x(n) A^n W^{n^2}$ and $y_2(n) = W^{-n^2}$, which in the spectral domain is realized as the product of the spectra of $Y_1(k)$ and $Y_2(k)$. The calculation of the CZT transform therefore requires three Fourier transforms to be determined: two simple and one inverse (Figure 6) [26,38–40].

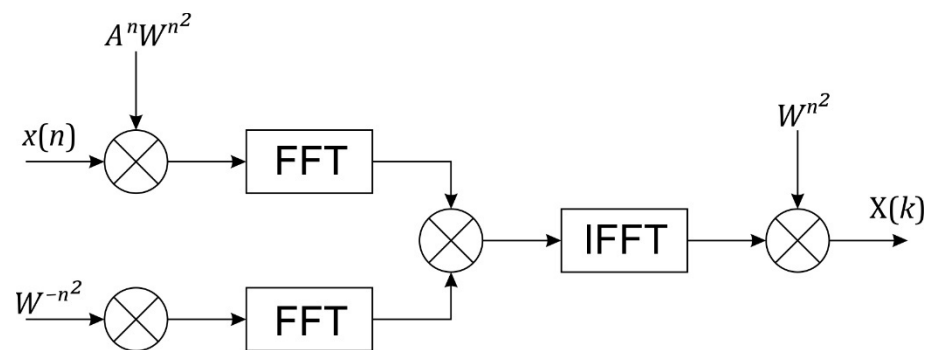


Figure 6. The block diagram of the determining the Chirp-Z transform.

4.2.1. Synthetic Signals Obtained by Decoding of the BMP File Subjected to the Differentiation Operation

The original Raster Generator application version1.0.2 was used to recreate the data and present them in the form of graphic images (Figure 7). The software has three basic modules:

- Graphic display and correction of rastering parameters;
- Low-pass, high-pass, median and edge detection;
- Signal analysis in time domain.

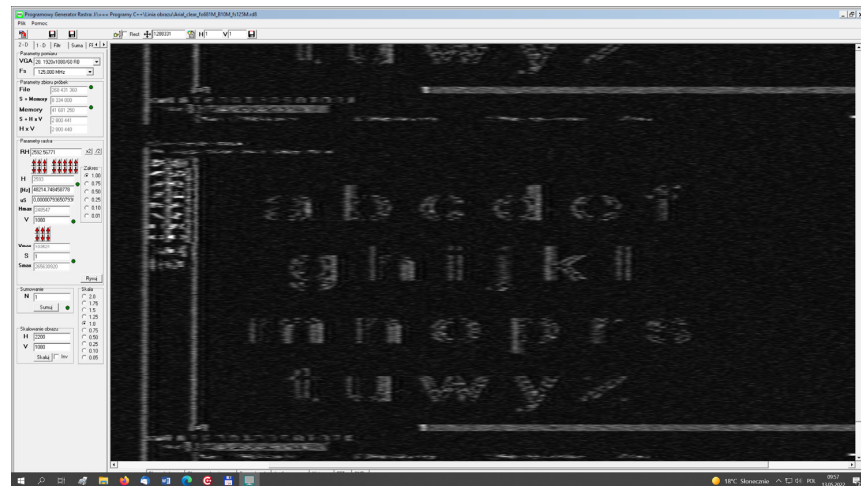


Figure 7. A window of Raster Generator with an exemplary reconstructed image based on a recorded revealing signal.

These allow the analysis of the emission signals, which are revealed for all sources of these emissions in the form of graphic lines (e.g., laser printers, computer monitors, graphic displays, graphic interfaces, etc.). The current version of the software enables manual estimation of rastering parameters in the absence of knowledge of the operating mode of the eavesdropped source of unwanted emissions. The estimation accuracy allows for efficient summing up to 60 replicas of the same image obtained from a single realization of the recorded revealing signal.

The signals described in point 3 (Figure 2) were used in the simulations. They show the test image often used in analyses of revealing emissions (Figure 2a) and the image of the MS Word application window used for text data processing. A differentiation of signals reflects the influence of an ideal information infiltration channel (Figure 8). For such images, an analysis of the accuracy of the line length estimation depending on the length of the transform (FFT and CZT) was conducted.

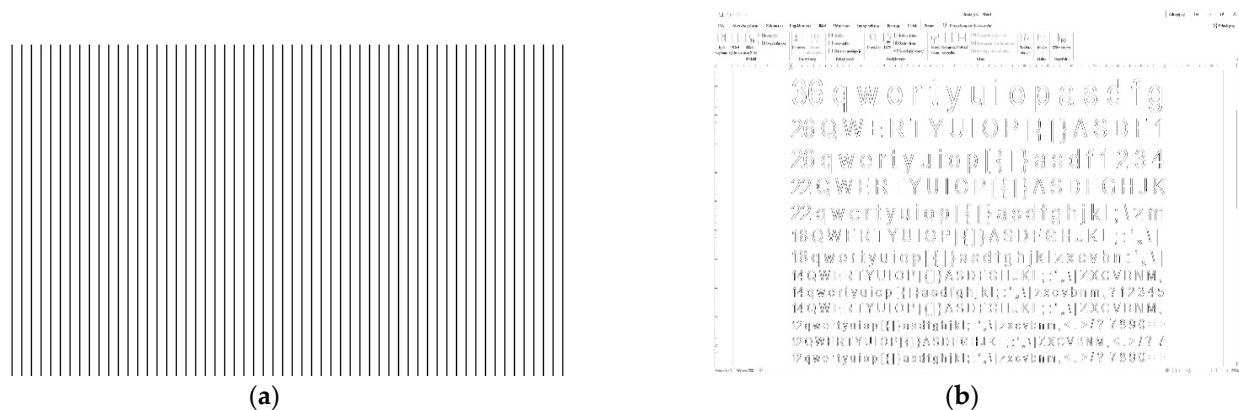


Figure 8. Rasterized images on base on test signals obtained from the BMP file after the differentiation operation: (a) strips 8×8 pixels-fragment, (b) window of MS Word editor.

The simulation results presented in Table 6 show that the precise estimation was obtained only for the test pattern in the form of vertical stripes (strict periodicity). The estimation for the MS Word test image is burdened with an error that has a significant impact on the image clarity after summation (Figure 9). Figure 9a,b present images after applying of 30-fold coherent summation. The line lengths of these images were estimated on the basis of analyzing the FFT algorithm (Table 6). The obtained results of line lengths are not the accurate values. Therefore, the summation of images does not improve the image quality. This phenomenon is shown on Figure 9, where reconstructed images

are blurred and illegible. However, this is typical of incorrect determination of raster parameters. Simultaneously, this points to a necessity to correct such parameters. Increasing the accuracy of the estimate requires the extension of the FFT transform. It can be concluded that satisfactory accuracy would be obtained with $N = 2^{27} = 134,217,728$.

Table 6. The simulation results for the test signals (differentiated images).

| Image | FFT Transform Length (N) | Chirp-Z Transform Length (N) | Real Line Length R_H | Designated Line Length R'_H | Estimation Inaccuracy $\Delta f_H = R_H - R'_H $ |
|--------------------------|--------------------------|------------------------------|------------------------|-------------------------------|---|
| Strips 8×8 | 2^{24} | 2^{22} | 2200 | 2200.000000 | 0.000000 |
| | 2^{24} | 2^{22} | | 2200.005559 | 0.005559 |
| Window of MS Word editor | 2^{25} | 2^{22} | | 2200.000629 | 0.000629 |
| | 2^{25} | 2^{23} | | 2200.000629 | 0.000629 |



Figure 9. Images reconstructed as a result of 30-fold summation for the R_H parameter defined for: (a) $N = 2^{24}$ (Table 6), (b) $N = 2^{25}$ (Table 6), according to the FFT algorithm.

4.2.2. Synthetic Signals Obtained by Decoding of the BMP File Subjected to the Differentiation Operation, Noisy by AWGN Noise

The next stage of the simulation for synthetic signals was estimating the R_H parameter for image signals subjected to the differentiation operation as well as noisy by white noise for the set SNR values: +15, +5.0, -5, -15 [dB]. A 10-fold estimation was conducted for each case (Table 7).

Table 7. Average values of the R_H parameter determined by the CZT method for synthetic signals (strips 8×8 , window of MS Word editor).

| Image | SNR [dB] | Real Line Length R_H | Designated Average Length of Line R'_H | Standard Deviation of the Estimate | Estimation Inaccuracy $\Delta f_H = R_H - R'_H $ |
|--------------------------|----------|------------------------|--|------------------------------------|---|
| Strips 8×8 | +15 | 2200 | 2200.000037 | 0.000107 | 0.000037 |
| | +5 | | 2199.999979 | 0.000434 | 0.000021 |
| | 0 | | 2200.000304 | 0.000593 | 0.000304 |
| | -5 | | 2200.000525 | 0.000915 | 0.000525 |
| | -15 | | 2199.999045 | 0.004018 | 0.000955 |
| Window of MS Word editor | +15 | 2200 | 2200.005539 | 0.000074 | 0.005539 |
| | +5 | | 2200.005534 | 0.000248 | 0.005534 |
| | 0 | | 2200.005702 | 0.000383 | 0.005702 |
| | -5 | | 2200.005146 | 0.001097 | 0.005146 |
| | -15 | | 2200.005560 | 0.002281 | 0.005560 |

In the case of differentiated signals, as well as noisy by AWGN noise $SNR < 0$, the accuracy of determining the rasterization parameters, especially in the case of the test image in the form of the MS Word editor window, is not sufficient to use them directly in the coherent summation process. The values should be more precise, e.g., on the basis of determining the measure of image clarity.

4.2.3. Signals Obtained by Sampling the Revealing Signal from the VGA Interface Received by the TEMPEST Test System DSI-1550 and Sampled by the ADC Card

Practical tests of the emission signals correlated with the information displayed on a computer monitor were carried out in the system shown in Figure 10. The computer set was placed in the shielding cabin on the measuring table. The tests used the TEMPEST Test System DSI-1550A measurement system (DSI-1550 RF Measurement System version 7.0.4.1 software) and a set of IZ1027A measurement antennas by Intriple: a vertical active rod antenna (100 Hz up to 50 MHz), a biconical active antenna (20 MHz up to 200 MHz), and a dipole active antenna (200 MHz up to 1000 MHz) with the IZ154B antenna switch (Figure 10). In order to sample the identified electromagnetic emission signals, a PDA-1000 8-bit analog-to-digital converter card, manufactured by Signatec (PDA100 Scope Application software, version 1.19), was used. The card offers a signal sampling rate of 1 GS/s, which may be reduced by using the card clock frequency division in the range from 2 to 1024.

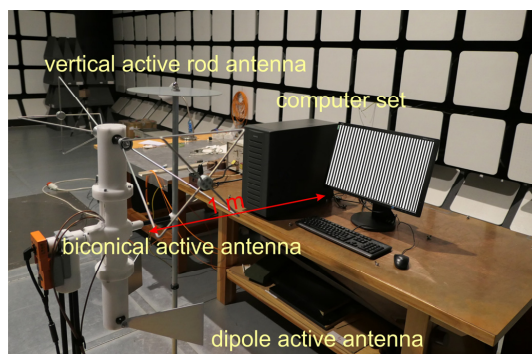


Figure 10. The real test system used to measure revealing emissions.

Using the test images (vertical 8×8 stripes and window of MS Word editor), the revealing signals of the line: graphics card-VGA cable-monitor, were recorded. The recording was performed at two reception frequencies: $f_o = 102$ MHz, where the strong emission from the cable was dominant, and $f_o = 424$ MHz, where the emission from the cable was suppressed. The signal was recorded using the sampling frequencies of the ADC card described in Section 2, in two reception bands: $B = 10$ and 20 [MHz]. The determined values of the R_H parameter were shown in Tables 8–10.

Table 8. Determination of the R_H parameter for the reception frequency $f_o = 102$ MHz, in the receiving band $BW = 10$ MHz, with the antenna amplifier on and off (+10 dB).

| Image | Receiving Bandwidth B [MHz] | Antenna Amplifier | Sampling Rate f_s [MS/s] | Real Line Length R_H | Designated Line Length R'_H | Estimation Inaccuracy $\Delta f_H = R_H - R'_H $ |
|---------------------|-------------------------------|-------------------|----------------------------|------------------------|-------------------------------|---|
| Strips 8×8 | 10 | ON | 62.5 | 925.920923 | 925.920893 | 0.000030 |
| | | | 125.0 | 1851.841761 | 1851.841520 | 0.000241 |
| | | | 250.0 | 3703.682958 | 3703.682158 | 0.000800 |
| | | | 500.0 | 7407.363841 | 7407.367141 | 0.003300 |
| | | OFF | 62.5 | 925.920829 | 925.921599 | 0.000770 |
| | | | 125.0 | 1851.841441 | 1851.246290 | 0.595151 |
| | | | 250.0 | 3703.682739 | 3703.688339 | 0.005600 |
| | | | 500.0 | 7407.364521 | 7406.767794 | 0.596727 |

Table 8. Cont.

| Image | Receiving Bandwidth B [MHz] | Antenna Amplifier | Sampling Rate f_s [MS/s] | Real Line Length R_H | Designated Line Length R'_H | Estimation Inaccuracy $\Delta f_H = R_H - R'_H $ |
|--------------------------|-------------------------------|-------------------|----------------------------|------------------------|-------------------------------|---|
| Window of MS Word editor | 20 | ON | 62.5 | 925.920800 | 927.568891 | 1.648091 |
| | | | 125.0 | 1851.841670 | 1855.146201 | 3.304531 |
| | | | 250.0 | 3703.682660 | 3710.223990 | 6.541330 |
| | | | 500.0 | 7407.363340 | 7420.748217 | 13.384877 |
| | | OFF | 62.5 | 925.920780 | 925.627822 | 0.292958 |
| | | | 125.0 | 1851.841480 | 1851.259880 | 0.581600 |
| | | | 250.0 | 3703.682520 | 3702.480226 | 1.202294 |
| | | | 500.0 | 7407.363950 | 7405.279559 | 2.084391 |

Table 9. Determination of the R_H parameter for the reception frequency $f_o = 102$ MHz, in the receiving band $BW = 20$ MHz, with the antenna amplifier on and off (+10 dB).

| Image | Receiving Bandwidth B [MHz] | Antenna Amplifier | Sampling Rate f_s [MS/s] | Real Line Length R_H | Designated Line Length R'_H | Estimation Inaccuracy $\Delta f_H = R_H - R'_H $ |
|--------------------------|-------------------------------|-------------------|----------------------------|------------------------|-------------------------------|---|
| Strips 8×8 | 20 | ON | 62.5 | 925.920869 | 925.920849 | 0.000020 |
| | | | 125.0 | 1851.841516 | 1851.841256 | 0.000260 |
| | | | 250.0 | 3703.682568 | 3703.680568 | 0.002000 |
| | | | 500.0 | 7407.363005 | 7407.357605 | 0.005400 |
| | | OFF | 62.5 | 925.920820 | 925.627866 | 0.292954 |
| | | | 125.0 | 1851.841510 | 1851.251144 | 0.590366 |
| | | | 250.0 | 3703.682600 | 3702.500522 | 1.182078 |
| | | | 500.0 | 7407.362820 | 7405.102352 | 2.260468 |
| Window of MS Word editor | 20 | ON | 62.5 | 925.920750 | 927.568714 | 1.647964 |
| | | | 125.0 | 1851.841350 | 1855.139643 | 3.298293 |
| | | | 250.0 | 3703.682400 | 3710.213356 | 6.530956 |
| | | | 500.0 | 7407.363260 | 7420.401191 | 13.037931 |
| | | OFF | 62.5 | 925.920800 | 925.627734 | 0.293066 |
| | | | 125.0 | 1851.841550 | 1851.261910 | 0.579640 |
| | | | 250.0 | 3703.682640 | 3702.481991 | 1.200649 |
| | | | 500.0 | 7407.364140 | 7404.390081 | 2.974059 |

Table 10. Determination of the R_H parameter for the reception frequency $f_o = 424$ MHz, in the receiving bands $BW = 10$ and 20 MHz, with the antenna amplifier on (+10 dB).

| Image | Receiving Bandwidth B [MHz] | Sampling Rate f_s [MS/s] | Real Line Length R_H | Designated Line Length R'_H | Estimation Inaccuracy $\Delta f_H = R_H - R'_H $ |
|---------------------|-------------------------------|----------------------------|------------------------|-------------------------------|---|
| Strips 8×8 | 10 | 62.5 | 925.623070 | 925.623145 | 0.000075 |
| | | 125.0 | 1851.246050 | 1851.245143 | 0.000907 |
| | | 250.0 | 3702.491410 | 3702.490815 | 0.000595 |
| | | 500.0 | 7404.981840 | 7405.057876 | 0.076036 |

Table 10. Cont.

| Image | Receiving Bandwidth B [MHz] | Sampling Rate f_s [MS/s] | Real Line Length R_H | Designated Line Length R'_H | Estimation Inaccuracy $\Delta f_H = R_H - R'_H $ |
|--------------------------|-------------------------------|----------------------------|------------------------|-------------------------------|---|
| Window of MS Word editor | 20 | 62.5 | 925.623100 | 925.623101 | 0.000001 |
| | | 125.0 | 1851.246230 | 1851.245408 | 0.000822 |
| | | 250.0 | 3702.492190 | 3702.492227 | 0.000037 |
| | | 500.0 | 7404.983240 | 7405.000339 | 0.017099 |
| | 10 | 62.5 | 925.623270 | 925.623454 | 0.000184 |
| | | 125.0 | 1851.246890 | 1851.246908 | 0.000018 |
| | | 250.0 | 3702.493120 | 3702.482520 | 0.010600 |
| | | 500.0 | 7404.985540 | 7404.916330 | 0.069210 |
| | 20 | 62.5 | 925.623420 | 925.623366 | 0.000054 |
| | | 125.0 | 1851.246740 | 1851.246290 | 0.000450 |
| | | 250.0 | 3702.493160 | 3702.493463 | 0.000303 |
| | | 500.0 | 7404.982540 | 7404.976336 | 0.006204 |

The use of the image rastering method in conjunction with the coherent summation method requires the geometrical dimensions of the reconstructed image to be determined (length and number of lines). Contemporary information display devices use resolutions for which the pixel frequency reaches values of 200 MHz. The sampling of the revealing emission signals resulting from the processing of such signals therefore requires the use of ADC converters capable of collecting at least 125 MS/s (taking into account letter size in ratio to pixel size). The experience of trying to reproduce images using the summation method shows that the length of the image line should be determined with an accuracy corresponding to the accuracy of determining the horizontal frequency of the order of 0.1 Hz. Taking into account the relationship (1), it is necessary to use the data set of 1.25 TS for the calculations. Since the FFT algorithms are optimized for sample sets with a multiplicity that is a multiple of 2, there is a need to perform calculations for a set of signal samples with a multiplicity of 2^{31} in the frequency range from 0 to $\frac{f_s}{2}$ Hz. The use of the Chirp-Z algorithm allows the search area to be narrowed to the frequency range concentrated around the searched value of the horizontal frequency, thus reducing the size of the sample set by a degree of about 4 to 8.

5. Conclusions

The article presents the preliminary results of the analysis of the possibility of using the Fourier and the CZT transforms to determine image rastering parameters in the process of electromagnetic infiltration. Particular attention was paid to the accuracy of determining the line length of the reconstructed image based on the accuracy of determining the value of the horizontal sync frequency of the eavesdropped display. The precision of the determination of the line length of the image is of great importance in the case of further processing of the reconstructed image, e.g., in accordance with the coherent summation algorithm to improve the SNR value. The results of the analyses presented in the article clearly show a significant advantage of using the FFT transform in the case when the critical parameter is the calculation time and the very ability to perform the calculations. The greater computational complexity of the CZT transform means that its calculation is at least a dozen times longer (e.g., for a data string with a length of 2^{22} , the FFT calculation time is 0.19 s for the Pentium C2Q Q8300 computer and 0.06 s for the Pentium i9-10900X computer, respectively); however, it is still a better approximation of the estimated line length of the reconstructed image. In the case of a data string with a length of 2^{25} , the

calculation times are 1.96 s and 0.43 s, respectively. Using the CZT transform under these conditions requires 2^{22} 15.26 s, 2.74 s and 298.82 s, 26.51 s for a data string of 2^{25} in length, respectively. After a fixed amount of RAM, the use of the FFT transform is possible for data strings of much longer length. The advantage of the CZT transform over the FFT transform consists of increasing the accuracy of calculations related to the narrowing of the frequency range under analysis. In the case of the ordinary FFT transform, its resolution defined by the formula (1) covers the entire range from 0 to $\frac{f_s}{2}$ Hz. However, in the case of the CZT transform, the resolution of the spectrum determination can be increased by performing the analysis only in the given frequency sub-range, with the accuracy defined by number of samples. The use of the CZT transform requires the knowledge of the limits of the analyzed frequency sub-range. Therefore, when determining the rasterization parameters of unknown signals, both transforms can be used together—FFT to roughly define the sought values F_H and F_V , and CZT to refine them. However, the use of the CZT transform requires the use of a hardware platform equipped with a significant amount of RAM, while the simulation results presented above indicate that even then the accuracy of the calculations may not be sufficient to obtain the raster parameter values that enable synchronous summation of signals corresponding to high-resolution images (Full HD and more). Therefore, the exact determination of the raster parameter values with the use of FFT and CZT transforms requires the use of additional mechanisms to refine these values using, for example, assessment measures of image quality. At a later stage of the work, it is planned to propose a measure of image quality assessment obtained on the basis of coherent summation and a criterion that will determine the acceptance of the image. Failure to meet the given criterion will force in further more accurate estimation of the image line length until the adopted criterion is met. For this, methods of the objective price of the images should be considered. The methods of objectively assessing the quality of visual content rely on the use of a computational algorithm, which, based on the analysis of visual content parameters, is able to approximate the average assessment that a given video sequence would obtain in the case of tests involving a group of testers. Due to the knowledge of the source information, the algorithms used in objective methods can be divided into three groups:

- Algorithms using full knowledge of the source information;
- Algorithms using limited knowledge of the source information;
- Algorithms without access to knowledge about source information.

The current methods of accepting of the determined values of the image line length and the number of lines in the image are based on visual assessment. Directly related to this is the ability to read graphic data contained in the reconstructed image. However, such a process is unacceptable due to the long time taken for the analysis of decision making. Automation of the process of determining basic rastering parameters is required. For this purpose, in a further stage of the research, measures and their acceptability criteria (image quality) will be proposed, which will allow for faster actions in the scope of determining the optimal line length and the number of lines in an image. Further work will focus on the analysis of the algorithm using full knowledge of the source information, i.e., sequences of high-quality visual content, and comparing this content with distorted content (the case that occurs in laboratory conditions during test device according to [41], which can process classified information). The measures that can be used to compare the reconstructed image with the reference image and which will be analyzed are:

- Mean Absolute Error (MAE);
- Mean Square Error (MSE) or its Root Mean Square Error (RMSE);
- Peak Signal to Noise Ratio (PSNR).

The described algorithm of line length estimation for the reconstructed images is extremely important for the effectiveness of the electromagnetic infiltration process and the assessment wireless communication devices from view point of their electromagnetic

immunity. This is related to the quality of the recorded electromagnetic emission signals, which are strongly noisy signals.

Author Contributions: Conceptualization, A.P.; methodology, A.P. and I.K.; software, A.P.; validation, I.K.; formal analysis, A.P. and I.K.; investigation, A.P.; resources, I.K.; data curation, A.P.; writing—original draft preparation, A.P. and I.K.; writing—review and editing, A.P. and I.K.; visualization, A.P. and I.K.; supervision, I.K.; project administration, A.P. and I.K. All authors have read and agreed to the published version of the manuscript.

Funding: This research received no external funding.

Institutional Review Board Statement: Not applicable.

Informed Consent Statement: Not applicable.

Data Availability Statement: Not applicable.

Conflicts of Interest: The authors declare no conflict of interest.

References

1. Boitan, A.; Bartusica, R.; Halunga, S.; Popescu, M.; Ionuta, I. Compromising Electromagnetic Emanations of Wired USB Keyboards. In Proceedings of the Third International Conference on Future Access Enablers for Ubiquitous and Intelligent Infrastructures (FABULOUS), Bucharest, Romania, 12–14 October 2017; Springer: Cham, Switzerland, 2017.
2. Zhang, N.; Yinghua, L.; Qiang, C.; Yiyang, W. Investigation of Unintentional Video Emanations from a VGA Connector in the Desktop Computers. *IEEE Trans. Electromagn. Compat.* **2017**, *59*, 1826–1834. [[CrossRef](#)]
3. Yuan, K.; Grassi, F.; Spadacini, G.; Pignari, S.A. Crosstalk-Sensitive Loops and Reconstruction Algorithms to Eavesdrop Digital Signals Transmitted Along Differential Interconnects. *IEEE Trans. Electromagn. Compat.* **2017**, *59*, 256–265. [[CrossRef](#)]
4. Kubiak, I. Laser printer as a source of sensitive emissions. *Turk. J. Electr. Eng. Comput. Sci.* **2018**, *26*, 1354–1366.
5. Kubiak, I.; Loughry, J. LED Arrays of Laser Printers as Valuable Sources of Electromagnetic Waves for Acquisition of Graphic Data. *Electronics* **2019**, *8*, 1078. [[CrossRef](#)]
6. Birukawa, R.; Hayashi, Y.; Mizuki, T.; Sone, H. A study on an Effective Evaluation Method for EM Information Leakage without Reconstructing Screen. In Proceedings of the International Symposium and Exhibition on Electromagnetic Compatibility (EMC Europe 2019), Barcelona, Spain, 2–6 September 2019.
7. *VESA and Industry Standards and Guidelines for Computer Display Monitor Timing (DMT)*; Version 1.0, Revision 13; 8 February 2013, 39899 Balentine Drive, Suite 125 Phone: 510 651 5122, Newark, CA 94560. Available online: <https://vesa.org/vesa-standards/> (accessed on 23 April 2022).
8. De Meulemeester, P.; Scheers, B.; Vandenbosch, G.A.E. Eavesdropping a (ultra-)high-definition video display from an 80 meter distance under realistic circumstances. In Proceedings of the 2020 IEEE International Symposium on Electromagnetic Compatibility & Signal/Power Integrity (EMCSI), Reno, NV, USA, 27–31 July 2021.
9. Levina, A.; Mostovoi, R.; Sleptsova, D.; Tsvetkov, L. Physical model of sensitive data leakage from PC-based cryptographic systems. *J. Cryptogr. Eng.* **2019**, *9*, 393–400. [[CrossRef](#)]
10. Trip, B.; Butnariu, V.; Vizitiu, M.; Boitan, A.; Halunga, S. Analysis of Compromising Video Disturbances through Power Line. *Sensors* **2022**, *22*, 267. [[CrossRef](#)]
11. Bartusica, R.; Boitan, A.; Fratu, O.; Mihai, M. Processing gain considerations on compromising emissions. In Proceedings of the Conference: Advanced Topics in Optoelectronics, Microelectronics and Nanotechnologies 2020, Constanta, Romania, 20–23 August 2020. [[CrossRef](#)]
12. Nowosielski, L.; Dudzinski, B.; Przesmycki, R.; Bugaj, M. Specifying Power Filter Insertion Loss Values in Terms of Electromagnetic Safety of IT Equipment. *Electronics* **2021**, *10*, 2041. [[CrossRef](#)]
13. Przybysz, A.; Grzesiak, K.; Kubiak, I. Electromagnetic Safety of Remote Communication Devices—Videoconference. *Symmetry* **2021**, *13*, 323. [[CrossRef](#)]
14. Choi, D.H.; Lee, E.; Yook, J.G. Reconstruction of Video Information Through Leaked Electromagnetic Waves from Two VDUs Using a Narrow Band-Pass Filter. *IEEE Access* **2022**, *10*, 40307–40315. [[CrossRef](#)]
15. De Meulemeester, P.; Scheers, B.; Vandenbosch, G.A.E. A quantitative approach to eavesdrop video display systems exploiting multiple electromagnetic leakage channels. *IEEE Trans. Electromagn. Compat.* **2020**, *62*, 663–672. [[CrossRef](#)]
16. Rubab, N.; Manzoor, N.; un Nisa, T.; Hussain, I.; Amin, M. Repair of video frames received by eavesdropping from VGA cable transmission. Processing of the 2018 15th International Bhurban Conference on Applied Sciences & Technology (IBCAST), Islamabad, Pakistan, 9–13 January 2018.
17. Maxwell, M.; Funlade, S.; Lauder, D. Unintentional Compromising Electromagnetic Emanations from IT Equipment: A Concept Map of Domain Knowledge. *Procedia Comput. Sci.* **2022**, *200*, 1432–1441.
18. Xueyun, H.; Xiaosong, L.; Yingping, Z.; Pengfei, Z.; Haohua, C.; Xiaonan, Z. Microstrip Bandstop Filter for Preventing Conduction Electromagnetic Information Leakage of High-Power Transmission Line. *Int. J. Antennas Propag.* **2022**, *2022*, 4915492. [[CrossRef](#)]

19. Popescu, M.; Bartusica, R. Aspects regarding the customized analysis of emission security risks for certain types of compromising signals. In Proceedings of the 2021 IEEE International Black Sea Conference on Communications and Networking (BlackSeaCo), Bucharest, Romania, 24–28 May 2021. [\[CrossRef\]](#)
20. Nowosielski, L. Impact of IT equipment location in buildings on electromagnetic safety. *Int. J. Electron. Telecommun.* **2020**, *66*, 481–486. [\[CrossRef\]](#)
21. Tajima, K.; Ishikawa, R.; Mori, T.; Suzuki, Y.; Takaya, K. A study on risk evaluation of countermeasure 284 technique for preventing electromagnetic information leakage from ITE. In Proceedings of the International Symposium on 285 Electromagnetic Compatibility (EMC Europe 2017), Angers, France, 4–8 September 2017.
22. Gyamfi, E.; Jurcut, A. Intrusion Detection in Internet of Things Systems: A Review on Design Approaches Leveraging Multi-Access Edge Computing, Machine Learning, and Datasets. *Sensors* **2022**, *22*, 3744. [\[CrossRef\]](#)
23. Ali, A.; Mateen, A.; Hanan, A.; Amin, F. Advanced Security Framework for Internet of Things (IoT). *Technologies* **2022**, *10*, 60. [\[CrossRef\]](#)
24. Aydın, H. TEMPEST Attacks and Cybersecurity. *Int. J. Eng. Technol.* **2019**, *5*, 100–104.
25. Sekiguchi, H. Information leakage of input operation on touch screen monitors caused by electromagnetic noise. In Proceedings of the IEEE International Symposium on Electromagnetic Compatibility, Fort Lauderdale, FL, USA, 25–30 July 2010. [\[CrossRef\]](#)
26. Zieliński, T.P. *Cyfrowe Przetwarzanie Sygnałów, od Teorii do Zastosowań*; Wydawnictwa Komunikacji Łączności (WKŁ): Warszawa, Poland, 2005.
27. Qin, M.; Li, D.; Tang, X.; Zeng, C.; Li, W.; Xu, L. A Fast High-Resolution Imaging Algorithm for Helicopter-Borne Rotating Array SAR Based on 2-D Chirp-Z Transform. *Remote Sens.* **2019**, *11*, 1669. [\[CrossRef\]](#)
28. Yang, W.; Chen, J.; Zeng, C.C.; Wang, P.B.; Liu, W. A Wide-Swath Spaceborne TOPS SAR Image Formation Algorithm Based on Chirp Scaling and Chirp-Z Transform. *Sensors* **2016**, *16*, 2095. [\[CrossRef\]](#)
29. Granados-Lieberman, D.; Romero-Troncoso, R.J.; Cabal-Yepez, E.; Osornio-Rios, R.A.; Franco-Gasca, L.A. A Real-Time Smart Sensor for High-Resolution Frequency Estimation in Power Systems. *Sensors* **2009**, *9*, 7412–7429. [\[CrossRef\]](#)
30. Kubiak, I. The Influence of the Structure of Useful Signal on the Efficacy of Sensitive Emission of Laser Printers. *Measurement* **2018**, *119*, 63–74. [\[CrossRef\]](#)
31. Kubiak, I. Influence of the method of colors on levels of electromagnetic emissions from video standards. *IEEE Trans. Electromagn. Compat.* **2018**, *61*, 1129–1137. [\[CrossRef\]](#)
32. Guri, M.; Elovici, Y. Exfiltration of information from air-gapped machines using monitor’s LED indicator. In Proceedings of the 2014 IEEE Joint Intelligence and Security Informatics Conference, Washington, DC, USA, 24–26 September 2014; pp. 264–267.
33. Hee-Kyung, L.; Yong-Hwa, K.; Young-Hoon, K.; Seong-Cheol, K. Emission Security Limits for Compromising Emanations Using Electromagnetic Emanation Security Channel Analysis. *IEICE Trans. Commun.* **2013**, *96*, 2639–2649.
34. Prvulovic, M.; Zajic, A.; Callan, R.L.; Wang, C.J. A Method for Finding Frequency-Modulated and Amplitude-Modulated Electromagnetic Emanations in Computer Systems. *IEEE Trans. Electromagn. Compat.* **2017**, *59*, 34–42. [\[CrossRef\]](#)
35. Ho Seong, L.; Jong-Gwan, Y.; Kyuhong, S. Analysis of information leakage from display devices with LCD. In Proceedings of the URSI Asia-Pacific Radio Science Conference 2016, Seoul, Korea, 21–25 August 2016.
36. Jun, S.; Yongacoglu, A.; Sun, D.; Dong, W. Computer LCD recognition based on the compromising emanations in cyclic frequency domain. In Proceedings of the IEEE International Symposium on Electromagnetic Compatibility, Ottawa, ON, Canada, 25–29 July 2016; pp. 164–169.
37. Song, T.L.; Jong-Gwan, J. Study of jamming countermeasure for electromagnetically leaked digital video signals. In Proceedings of the IEEE International Symposium on Electromagnetic Compatibility, Gothenburg, Sweden, 1–4 September 2014. [\[CrossRef\]](#)
38. Rabiner, L.; Schafer, R.; Rader, C. The Chirp-Z transform algorithm. *IEEE Trans. Audio Electroacoust.* **1969**, *17*, 86–92. [\[CrossRef\]](#)
39. Aiello, M.; Cataliotti, A.; Nuccio, S. A Chirp-Z transform-based synchronizer for power system measurements. *IEEE Trans. Instrum. Meas.* **2005**, *54*, 1025–1032. [\[CrossRef\]](#)
40. Draidi, J.A. Two-dimensional Chirp-Z transform and its application to zoom Wigner bispectrum. In Proceedings of the IEEE International Symposium on Circuits and Systems (ISCAS 96), Atlanta, GA, USA, 15 May 1996.
41. SDIP-27/2-Tempest Requirements and Evaluation Procedures (published as AC/322-D(2016)0022), NATO Confidential, 20 March 2016, *accepted*.